TRIP13 localizes to synapsed chromosomes and functions as a dosage-sensitive regulator of meiosis

Jessica Y. Chotiner[1], N. Adrian Leu[1], Fang Yang[1], Isabella G. Cossu[1], Yongjuan Guan[1,2], Huijuan Lin[1], and P. Jeremy Wang[1],*

[1]Department of Biomedical Sciences, University of Pennsylvania School of Veterinary Medicine, Philadelphia, PA 19104, USA. [2]College of Life Sciences, Capital Normal University, Beijing, China.

*For correspondence: pwang@vet.upenn.edu

Abstract

Meiotic progression requires coordinated assembly and disassembly of protein complexes involved in chromosome synapsis and meiotic recombination. The AAA+ ATPase TRIP13 and its orthologue Pch2 are instrumental in remodeling HORMA domain proteins. Meiosis-specific HORMAD proteins are associated with unsynapsed chromosome axes but depleted from the synaptonemal complex (SC) of synapsed chromosome homologues. Here we report that TRIP13 localizes to the synapsed SC in early pachytene spermatocytes and to telomeres throughout meiotic prophase I. Loss of TRIP13 leads to meiotic arrest and thus sterility in both sexes. *Trip13*-null meiocytes exhibit abnormal persistence of HORMAD1 and HOMRAD2 on synapsed SC and chromosome asynapsis that preferentially affects XY and centromeric ends. *Trip13* heterozygous (*Trip13*$^{+/-}$) mice also exhibit meiotic defects that are less severe than the *Trip13*-null mice, showing that TRIP13 is a dosage-sensitive regulator of meiosis. Localization of TRIP13 to the synapsed SC is independent of SC axial element proteins such as REC8 and SYCP2/SYCP3. The N- or C-terminal FLAG tagged TRIP13 proteins are functional and recapitulate the localization of native TRIP13 to SC and telomeres in knockin mice. Therefore, the evolutionarily conserved localization of TRIP13/Pch2 to the synapsed chromosomes provides a spatial explanation for dissociation of HORMA domain proteins upon chromosome synapsis in diverse organisms.

Introduction

Meiosis is a specialized cell division program that generates haploid gametes from diploid germ cells. During meiotic prophase I, homologous chromosomes undergo paring, synapsis, and recombination (Handel and Schimenti, 2010; Zickler and Kleckner, 2015). Chromosome synapsis requires the formation of the synaptonemal complex (SC). The SC is a proteinaceous structure comprised of two lateral/axial elements, transverse filaments, and a central element (Page and Hawley, 2004). Meiotic recombination begins with generation of DNA double strand breaks (DSBs) and ends with crossover formation through repair of DSBs (Hunter, 2015). Chromosome synapsis and meiotic recombination are interdependent in many species including yeast and mouse. Meiotic recombination not only increases genetic diversity in gametes at the organism level but also is essential for faithful chromosome segregation during the first meiotic cell division. Therefore, defects in meiosis are leading causes of aneuploidy, birth defect, infertility, and pregnancy loss.

The progression and completion of synapsis and recombination are monitored by a surveillance mechanism called meiotic checkpoint (Roeder and Bailis, 2000). Meiotic checkpoint proteins were extensively studied in yeast. Many meiotic processes are highly conserved, and studies of meiosis in yeast have been foundational for our understanding of mammalian meiosis. In yeast, Pch2, an AAA+ ATPase,

46 is a checkpoint protein, because it is necessary for pachytene arrest in the absence of the SC protein Zip1
47 or the meiosis-specific DSB repair protein Dmc1 (Herruzo et al., 2021; San-Segundo and Roeder, 1999).
48 Pch2 is a hexameric ring ATPase and remodels the HORMA (Hop1, Rev7, and MAD2) domain protein
49 Hop1 in a nucleotide-dependent manner (Chen et al., 2014). While Pch2 is mainly located in the
50 nucleolus, Pch2 also localizes to the synapsed SC as foci at the pachytene stage and is essential for
51 removing Hop1 from chromosome axes (Chen et al., 2014; Joshi et al., 2009; San-Segundo and Roeder,
52 1999). Mechanistically, Pch2 promotes phosphorylation of Hop1, which activates the Mek1 kinase and
53 the subsequent checkpoint cascade (Herruzo et al., 2016; Raina and Vader, 2020).
54 TRIP13, the mammalian orthologue of yeast Pch2, is essential for completion of meiotic
55 recombination in mouse (Li and Schimenti, 2007; Roig et al., 2010). Mutations in human *TRIP13*
56 predispose to Wilms tumor in children or cause infertility in women (Yost et al., 2017; Zhang et al.,
57 2020). HORMAD1 and HORMAD2, mammalian meiosis-specific HORMA domain proteins, localize to
58 chromosome axis at leptotene and zygotene stages but are depleted from synapsed chromosomes except
59 the largely unsynapsed XY chromosomes at the pachytene stage (Fukuda et al., 2010; Xu et al., 2019).
60 TRIP13 facilitates removal of HORMAD proteins from synapsed chromosome axis (Roig et al., 2010;
61 Wojtasz et al., 2009). SKP1, an essential component of the SCF (Skp1-Cullin 1-F-box protein) ubiquitin
62 E3 ligase, is required not only for depleting HORMAD1 and HORMAD2 from synapsed chromosome
63 axes but also for restricting the accumulation of HORMAD proteins on unsynapsed axes (Guan et al.,
64 2020; Guan et al., 2022). Therefore, reorganization of HORMA domain proteins on meiotic chromosome
65 axes is regulated by both TRIP13 and SKP1. As a conserved mechanism, Pch2/TRIP13 remodels
66 HORMA domain proteins through engagement of their N-terminal regions (Prince and Martinez-Perez,
67 2022). MAD2, a spindle assembly checkpoint HORMA domain protein, exists in two fold states: closed
68 and open (Luo et al., 2004; Sironi et al., 2002). In the closed state, the so-called safety belt of the
69 HORMA domain wraps around the HORMAD protein-binding motif "closure motif" in the partner
70 protein and thus traps the partner. In the open state, TRIP13 engagement changes conformation of the
71 HORMA domain, resulting in foldback of the safety belt on the closure motif-binding region and thus
72 release of its partner protein. The safety belt mechanism turns out to be a shared feature of HORMA
73 domain proteins (Kim et al., 2014; West et al., 2019; West et al., 2018; Ye et al., 2017).
74 Unlike yeast Pch2, TRIP13 does not appear to function in the meiotic checkpoint in mouse
75 (Pacheco et al., 2015). Interestingly, HORMAD2 functions as a meiotic checkpoint protein for
76 surveillance of meiotic defects in female meiosis (Kogo et al., 2012a; Rinaldi et al., 2017; Wojtasz et al.,
77 2012). HORMAD2-deficient males are sterile but females are fertile. HORMAD2 deficiency rescues the
78 oocyte loss in *Spo11*-null or *Trip13* mutant females but not in *Dmc1*-null females, suggesting that

79 HORMAD2 is a component of the meiotic checkpoint in females. HORMAD1 is required for fertility in
80 both sexes (Kogo et al., 2012b; Shin et al., 2010; Stanzione et al., 2016). Both HORMAD1 and
81 HORMAD2 localize prominently to the XY chromosome axes in pachytene spermatocytes and regulate
82 meiotic sex chromatin inactivation (MSCI) (Kogo et al., 2012a; Shin et al., 2010; Wojtasz et al., 2012).
83 Studies of mice with hypomorphic *Trip13* mutations show that TRIP13 is required for meiotic
84 progression (Li and Schimenti, 2007; Roig et al., 2010). Two different hypomorphic *Trip13* mouse lines
85 have been studied: one "moderate" allele that exhibited defective meiotic recombination and one "severe"
86 allele that displayed defects in meiotic recombination and chromosome synapsis. The variance in
87 phenotype between the hypomorphic mouse lines indicates that even partial depletion of *Trip13* can
88 interrupt meiosis. We sought to further investigate the meiotic function of TRIP13. By
89 immunofluorescence, we found that TRIP13 localized to the synaptonemal complex in early pachytene
90 spermatocytes and to telomeres throughout meiotic prophase I. The TRIP13 localization pattern on
91 meiotic chromosomes was further confirmed by analysis of FLAG-tagged TRIP13 in two knockin mouse
92 lines. We characterized *Trip13*-null mice. While the *Trip13*-null phenotype was largely comparable to the
93 phenotype of the severe *Trip13* hypomorphic allele, we found that TRIP13 is a dosage-sensitive regulator
94 of meiosis. Finally, our results show that the localization of TRIP13 to the SC is independent of axial
95 element proteins.
96
97 **Results**
98
99 **TRIP13 localizes to meiotic chromosomes in prophase I spermatocytes**
100 We assessed the expression of TRIP13 in a panel of adult mouse tissues. TRIP13 was primarily expressed
101 in testis but detected at low levels in ovary and liver (Figure 1A). In the testis, TRIP13 was prominent in
102 the cytoplasm of primary spermatocytes, especially leptotene and zygotene cells (Figure 1B). Given the
103 expression of TRIP13 in spermatocytes, we examined its localization on meiotic chromosomes by
104 immunostaining of surface spread nuclei of prophase I spermatocytes (Figure 1C). Previously, TRIP13
105 was reported to localize to telomeres in spermatocytes (Gomez et al., 2019). Indeed, we found that
106 TRIP13 localized to telomeres from leptotene to diplotene cells (Figure 1C). Strikingly, we found that, in
107 addition to telomeres, TRIP13 localized to the synaptonemal complex (SC) in early pachytene
108 spermatocytes but disappeared from the SC in the mid to late pachytene spermatocytes (Figure 1C). The
109 synaptonemal complex consists of two lateral elements and one central element. The central region is
110 comprised of the transverse filament protein SYCP1 and central element proteins, which appear upon
111 synapsis. Given the novel localization of TRIP13 to the SC, we performed confocal immunofluorescent

112 microscopy with super-resolution deconvolution to determine the location of TRIP13 within the SC. In
113 contrast with the lateral element marker SYCP3, TRIP13 localized to the SC central region (Figure 1D).
114 We examined the localization of TRIP13 in oocytes. TRIP13 localized strongly to meiotic telomeres in all
115 stages of prophase I, but not as filaments on the SC (Figure 1 - figure supplement 1). These findings are
116 consistent with the genetic requirement of TRIP13 in meiosis in both sexes (Li and Schimenti, 2007; Roig
117 et al., 2010).
118
119 **Global loss of *Trip13* causes meiotic arrest**
120 Two previous studies utilizing two *Trip13* hypomorphic (gene trap) alleles, one moderate and one severe,
121 revealed a role for TRIP13 in meiotic recombination (Li and Schimenti, 2007; Roig et al., 2010).
122 However, while the *Trip13* moderate allele showed mostly intact chromosomal synapsis, the severe allele
123 displayed chromosomal unsynapsis preferentially at chromosome ends (Li and Schimenti, 2007; Roig et
124 al., 2010). Upon close examination, we also found unsynapsed ends in spermatocytes with the moderate
125 *Trip13* mutant (Guan et al., 2020). To rigorously ascertain the role of TRIP13 in meiosis, we generated
126 *Trip13*-null mutants using frozen sperm from *Trip13*$^{+/-}$ males with a knockout allele from the
127 International Mouse Phenotyping Consortium (IMPC). The mouse *Trip13* gene consists of 13 exons. This
128 new *Trip13* mutant allele harbors a deletion of a 24-kb region including all 13 exons and thus is expected
129 to be null. We verified this deletion by PCR and sequencing. Interbreeding of *Trip13*$^{+/-}$ mice produced
130 fewer *Trip13*$^{-/-}$ offspring than expected: *Trip13*$^{+/+}$, 80; *Trip13*$^{+/-}$, 220; *Trip13*$^{-/-}$, 51 ($\chi 2$=27, p=0.0001). The
131 *Trip13*$^{-/-}$ testis was much smaller than *Trip13*$^{+/-}$ testis (Figure 2A). Western blot analysis showed that
132 TRIP13 was present in reduced abundance in *Trip13*$^{+/-}$ testis and not detected in *Trip13*$^{-/-}$ testis,
133 demonstrating that this mutant allele is null (Figure 2B). The abundance of SYCP3, a component of the
134 synaptonemal complex, was also reduced in *Trip13*$^{-/-}$ testis, suggesting a partial depletion of meiotic cells
135 (Figure 2B). The testis weight of adult *Trip13*$^{-/-}$ males was reduced by 74% in comparison with the wild
136 type males (Figure 2C). Adult *Trip13*$^{-/-}$ males lacked sperm in the epididymis (Figure 2D). Histological
137 analysis showed that while spermatocytes in all stages of meiosis were present in adult *Trip13*$^{+/+}$ and
138 *Trip13*$^{+/-}$ testes, *Trip13*$^{-/-}$ testis displayed complete meiotic arrest, evidenced by the presence of early
139 spermatocytes and a lack of secondary spermatocytes, round spermatids, and mature sperm (Figure 2E).
140 *Trip13*$^{-/-}$ females were also sterile. The adult *Trip13*$^{-/-}$ ovary was very small and showed a complete loss
141 of oocytes (Figure 2 - figure supplement 1). These observations are similar to the meiotic arrest phenotype
142 observed in the hypomorphic *Trip13* mouse mutants (Li and Schimenti, 2007; Roig et al., 2010).
143
144 **Defects in chromosomal synapsis in *Trip13*-deficient spermatocytes**

145 We investigated the effect of *Trip13* deficiency on meiotic progression. The transverse filament/central
146 element protein SYCP1 and the lateral element protein SYCP3 were used to determine the stage of
147 prophase I spermatocytes. While the P20 wild type testis contained spermatocytes from leptotene through
148 diplotene stages, about half of the *Trip13*$^{-/-}$ spermatocytes were in the early pachytene stage and no cells
149 were found at later stages of prophase I, showing meiotic blockade at the early pachytene stage in *Trip13*$^{-}$
150 $^{/-}$ testes (Figure 3A). The early pachytene-like spermatocytes from *Trip13*$^{-/-}$ testes contained unsynapsed
151 chromosomal ends (Figure 3B). Mouse centromeres are telocentric. Co-staining with the centromere
152 marker CREST showed that 94% of unsynapsed ends were centromeric ends (Figure 4A). While XY
153 chromosomes were synapsed at the pseudoautosomal regions and thus were connected in wild type and
154 *Trip13*$^{+/-}$ pachytene spermatocytes, they were separate in *Trip13*$^{-/-}$ pachytene-like spermatocytes (Figure
155 3B and Figure 3C). We found that SYCE1, a component of the SC central element, localized to the
156 synapsed SC but not to unsynapsed regions in *Trip13*$^{-/-}$ pachytene-like cells (Figure 3C). Confocal
157 microscopy with super-resolution deconvolution confirmed that many homologous chromosomes in
158 *Trip13*$^{-/-}$ spermatocytes had split ends and some had regions of interstitial asynapsis (Figure 3D). We
159 quantified these meiotic defects in spermatocytes: chromosomal asynapsis (Figure 3E), the number of
160 asynapsed ends (Figure 3F), and the extent of XY asynapsis (Figure 3G). Previous studies also reported
161 synaptic defects in spermatocytes from *Trip13* hypomorph mutants (Li and Schimenti, 2007; Roig et al.,
162 2010). Here we found that global loss of *Trip13* caused similar defects in autosomal synapsis but a more
163 severe defect in sex chromosome synapsis.
164
165 **TRIP13 is a dosage-sensitive regulator of meiosis**
166 Although *Trip13*$^{+/-}$ males were fertile, their testis weight and sperm count were significantly reduced in
167 comparison with wild type (Figure 2C-D). The percentage of spermatocytes with defects in synapsis was
168 higher in *Trip13*$^{+/-}$ males than wild type (Figure 3E). In addition, the percentage of spermatocytes with
169 asynapsed XY chromosomes was significantly higher in *Trip13*$^{+/-}$ males than wild type (Figure 3G). As
170 defects in synapsis can activate the meiotic checkpoint and thus apoptosis of affected spermatocytes, the
171 increased synaptic defects likely caused the decrease in sperm output in *Trip13*$^{+/-}$ males. These results
172 demonstrate that TRIP13 regulates meiosis in a dosage-dependent manner.
173
174 **Telomere and centromere proteins localize normally in *Trip13*-deficient spermatocytes**
175 TRIP13 localizes to telomeres and loss of TRIP13 causes peri-centromeric/telomeric asynapsis.
176 Therefore, we asked whether telomere or centromere proteins were affected in *Trip13*$^{-/-}$ spermatocytes.
177 Chromosome spreads were immunostained for two centromere markers, CREST and CENPC (Figure 4A-

178 B). CENPC is essential for recruiting kinetochore proteins to the centromere (Klare et al., 2015; Kwon et
179 al., 2007). CREST and CENPC still localized to centromeres in *Trip13*$^{-/-}$ spermatocytes. Because many
180 *Trip13*$^{-/-}$ spermatocytes had split ends, two CREST or two CENPC foci were observed at the split ends.
181 To assess the telomere, spermatocytes were immunostained for TRF1 and MAJIN (Figure 4C-D). In
182 meiotic cells, telomeres contain canonical telomere proteins such as TRF1/TRF2 and a meiosis-specific
183 complex (MAJIN, TERB1, TERB2, and SUN1) (Shibuya et al., 2015). TRF1 is a telomere protein
184 expressed in both somatic and germ cells (Karlseder et al., 2003; Long et al., 2017; Shibuya et al., 2014).
185 MAJIN is a component of the meiosis-specific telomere complex that is important for telomere
186 attachment to the inner nuclear membrane (Shibuya et al., 2015). Both TRF1 and MAJIN localized to
187 telomeres in *Trip13*$^{-/-}$ spermatocytes (Figure 4C-D). Taken together, these results suggest that TRIP13 is
188 not required for recruitment of these centromere or telomere proteins.
189
190 **TRIP13 is required to evict HORMAD1 and HORMAD2 from synapsed autosomes**
191 In wild type meiotic cells, HORMAD1 and HORMAD2 localize to unsynapsed and desynapsed
192 chromosomes (Fukuda et al., 2010; Kogo et al., 2012a; Shin et al., 2010; Wojtasz et al., 2012). Thus,
193 HORMAD1 and HORMAD2 localized to the largely unsynapsed XY but not to synapsed autosomal SCs
194 in wild type cells (Figure 5A-B). TRIP13 is essential for removing meiotic HORMADs from the
195 chromosome axes, a function that is conserved in yeast, worms, and mammals (Wojtasz et al., 2009). We
196 confirmed that HORMAD1 and HORMAD2 remained on the synapsed autosomes in *Trip13*$^{-/-}$ pachytene
197 cells (Figure 5A-B). HORMAD1 and HORMAD2 localize to the interior of the lateral elements in the SC
198 (Xu et al., 2019). Confocal microscopy with super-resolution deconvolution revealed that HORMAD1
199 and HORMAD2 localized to the lateral elements of the synapsed autosomes in *Trip13*$^{-/-}$ spermatocytes
200 (Figure 5C-D). These results were consistent with accumulation of HORMAD1/2 in *Trip13* hypomorphic
201 mutant spermatocytes (Roig et al., 2010; Wojtasz et al., 2009). Our analysis of *Trip13*-null mutant
202 confirmed that TRIP13 is essential for HORMAD1/2 removal from the synapsed SCs.
203
204 **Localization of TRIP13 to SC is independent of axial element components**
205 TRRIP13 localizes to the SC in early pachytene spermatocytes. We sought to address what proteins might
206 recruit TRIP13 to the SC. We examined the role of HORMAD1, REC8, SYCP2, and SKP1 in TRIP13
207 localization in spermatocytes using respective knockout mice (Figure 6). We first examined the
208 localization of TRIP13 in *Hormad1*$^{-/-}$ spermatocytes. *Hormad1*$^{-/-}$ spermatocytes exhibit limited synapsis
209 (Daniel et al., 2011; Kogo et al., 2012b; Shin et al., 2010). In both wild type and *Hormad1*$^{-/-}$ cells, TRIP13

210 localized to the synapsed regions and to the telomeres (Figure 6A). This result shows that HORMAD1 is
211 not required for localization of TRIP13 to the SC.
212 REC8, a meiosis-specific cohesin, promotes synapsis between homologs and inhibits synapsis
213 between sister chromatids (Xu et al., 2005). In the absence of REC8, synapsis occurs between sister
214 chromatids rather than homologous chromosomes. In *Rec8*$^{-/-}$ spermatocytes, TRIP13 localized to
215 synapsed sister chromatids (Figure 6B). To further probe TRIP13 recruitment to the SC, a mouse line
216 expressing a truncated SYCP2 was used (Yang et al., 2006). SYCP2 and SYCP3 are essential components
217 of the axial/lateral elements of the SC and interact with each other. The mutant used in this study (referred
218 to as *Sycp2*$^{-/-}$) expresses a truncated SYCP2 protein that lacks the C-terminal coiled-coil domain necessary
219 for binding to SYCP3. Thus, SYCP3 failed to localize to the axial elements and formed aggregates in
220 *Sycp2*$^{-/-}$ spermatocytes (Figure 6C). Nevertheless, *Sycp2*$^{-/-}$ spermatocytes formed short stretches of
221 synapsis (Figure 6C). TRIP13 localized as filaments in *Sycp2*$^{-/-}$ spermatocytes, strongly suggesting that its
222 localization is independent of SYCP3 and the C-terminus of SYCP2 (Figure 6C).
223 Previous work has shown that SKP1, a key component of the SKP1, Cullin, F-box (SCF) complex
224 E3 ligase, is important for HORMAD removal and chromosomal synapsis (Guan et al., 2020; Guan et al.,
225 2022). SKP1 localizes to synapsed regions in meiotic germ cells and specifically to the lateral elements in
226 the SC (Guan et al., 2020). We found that TRIP13 still localized to the synapsed regions in *Skp1*^{cKO}
227 (conditional knockout) spermatocytes (Figure 6D). Taken together, these results show that the SC
228 localization of TRIP13 is independent of HORMAD1, REC8, SYCP2, SYCP3, and SKP1, which all
229 localize to the SC lateral elements. Such a finding is consistent with the localization of TRIP13 to the SC
230 central region (Figure 1D).
231
232 **FLAG-tagged TRIP13 proteins are functional**
233 In order to investigate the mechanism of TRIP13 recruitment to the SC, we generated 3×FLAG-TRIP13
234 (N-terminal tag) and TRIP13-3×FLAG (C-terminal tag) mice through the CRISPR/Cas9-medidated
235 genome editing approach (Figure 7 - figure supplement 1). Two different types of tagged mice were
236 generated in case that one fusion protein is not functional. Both alleles were transmitted through the
237 germline of the founder mice. Western blot showed that TRIP13 existed in two isoforms in wild type
238 (non-tagged) testis (Figure 7A). The major TRIP13 isoform was 50 kDa. The minor isoform was slightly
239 larger than 50 kDa. Western blot analysis showed that the FLAG tagged TRIP13 fusion proteins were
240 present in both FLAG-tagged testes. Both FLAG-tagged TRIP13 fusion proteins also existed in two
241 isoforms in the homozygous testes, suggesting that they corresponded to the two wild type isoforms. The
242 3×FLAG-TRIP13 proteins were apparently slightly larger, possibly due to the linker in the N-terminally

243 tagged proteins. The nature and physiological significance of these two isoforms were not clear, but could
244 be due to post-translational modification or alternative splicing. Immunofluorescence analysis using anti-
245 FLAG antibody showed that the FLAG tagged TRIP13 proteins, like wild type TRIP13, localized to both
246 telomeres and synaptonemal complex in pachytene spermatocytes from both FLAG/FLAG homozygous
247 testes (Figure 7B). Importantly, both N- and C-terminally tagged homozygous mice were fertile. These
248 results demonstrate that both N- and C-terminal tagged TRIP13 proteins localize normally and are
249 functional.

250 To identify TRIP13-associated proteins in testis, we performed immunoprecipitation (IP) using
251 3×FLAG-TRIP13, TRIP13-3×FLAG, and wild type (no tag) testicular protein extracts with anti-FLAG
252 monoclonal antibody. The immunoprecipitated proteins were eluted with FLAG peptides and subjected to
253 mass spectrometry for protein identification. As expected, TRIP13 had more peptides in tagged TRIP13
254 IP than wild type (Table 1). HORMAD2, a known TRIP13 substrate protein, was also enriched in tagged
255 TRIP13 IP (Table 1). Intriguingly, a large number of RNA-binding proteins involved in RNA splicing
256 were highly enriched in tagged TRIP13 IP: DDX46, PUF60, RBM25, RBM39, U2AF1, U2AF2, and
257 SRSF11 (Table 1). The biological relevance of these RNA-binding proteins to TRIP13 function remains
258 unknown. We cannot exclude the possibility that identification of these RNA splicing factors could be
259 immunoprecipitation artifacts.
260

261 **Discussion**

262 TRIP13 and its orthologue Pch2 play an evolutionarily conserved role in depletion of meiosis-specific
263 HORMA domain proteins from the synaptonemal complex in many species including yeast, plant, and
264 mouse. In meiocytes, HORMA domain proteins are associated with unsynapsed chromosome axes and
265 become depleted from the SC upon synapsis. In mice with *Trip13* hypomorphic gene trap alleles,
266 HORMAD1 and HORMAD2 persist on the synapsed SCs at the pachytene stage (Wojtasz et al., 2009). In
267 this study, we confirmed the abnormal persistence of HORMAD1 and HORMAD2 in *Trip13*-null
268 spermatocytes. In budding yeast, deficiency of Pch2 leads to accumulation of Hop1 on the SC (Joshi et
269 al., 2009; Subramanian et al., 2016). In *Arabidopsis*, Pch2 remodels the HORMA domain protein ASY1
270 (Balboni et al., 2020; Yang et al., 2020). Pch2 has been shown to localize to synapsed SC in budding
271 yeast (Joshi et al., 2009), C. elegans (Deshong et al., 2014; Russo et al., 2023), *Arabidopsis* (Lambing et
272 al., 2015), and rice (Miao et al., 2013), but not in mouse. In mouse meiocytes, TRIP13 was known to
273 localize to telomeres (Gomez et al., 2019). In addition to telomeres, we find that TRIP13 localizes to the
274 SC in early pachytene spermatocytes in mouse. In particular, TRIP13 localizes as a single filament
275 between the SC lateral elements. Therefore, TRIP13/Pch2 and HORMA domain proteins have mutually

276 exclusive localization patterns on the meiotic chromosome axes, providing a spatial explanation for the
277 depletion of HORMA domain proteins from the synapsed chromosomes in diverse organisms.
278 The transverse filaments (TF) are essential for recruitment of Pch2 to the SC. In a budding yeast
279 Zip1 (encoding the TF component) allele with four amino acid substitutions, Pch2 is absent from the SC
280 (Subramanian et al., 2016). In *C. elegans*, the TF component SYP-1 is essential for localization of Pch-2
281 on the paired chromosomes (Deshong et al., 2014). In rice, CRC1 (Pch2 orthologue) and CEP1 (TF
282 protein) localize to the SC in an inter-dependent manner (Miao et al., 2013). In *Arabidopsis*, ZYP1 (TF
283 component) recruits Pch2 to the SC (Yang et al., 2022). In the yeast two-hybrid assay, rice CRC1
284 interacts with CEP1, *Arabidopsis* ZYP1 interacts with Pch2, and mouse SYCP1 (TF protein) interacts
285 with TRIP13 (Miao et al., 2013; Yang et al., 2022). Unlike in other species, loss of SYCP1 (TF protein) in
286 mouse leads to a complete failure in chromosomal synapsis and thus its role in recruitment of TRIP13 to
287 the synapsed SC can not be directly addressed (de Vries et al., 2005). Our findings on the localization of
288 mouse TRIP13 to the SC on the sister chromatids in *Rec8*-deficient spermatocytes and the short SC
289 stretches in *Sycp2* mutant spermatocytes demonstrate that TRIP13 recruitment is independent of SC axial
290 element proteins REC8 and SYCP2 but support the possibility that SYCP1 could recruit TRIP13 to the
291 synapsed SC. These findings lead to the following model: the TF protein recruits Pch2/TRIP13 to the SC
292 upon synapsis, which in turn evicts HORMA domain proteins from the synapsed regions.
293 Both TRIP13 and SKP1 are required for removal of HORMA domain proteins from the synapsed
294 SC (Guan et al., 2020; Wojtasz et al., 2009). However, the relationship of TRIP13 and SKP1 is unknown.
295 SKP1 localizes to the synapsed SC more extensively than TRIP13. While TRIP13 is only detected on the
296 synapsed SC in early pachytene spermatocytes (Figure 1), SKP1 localizes to the synapsed SC in zygotene,
297 all stages of pachytene, and diplotene spermatocytes (Guan et al., 2020). The localization of TRIP13 and
298 SKP1 within the SC is different: TRIP13 is on CE/TF regions but SKP1 on LEs. While the global level of
299 TRIP13 is reduced in *Skp1*-deficient testes, the localization of TRIP13 and SKP1 to the synapsed SC is
300 independent (Figure 6D) (Guan et al., 2020). The SCF ubiquitin E3 ligase complex targets HORMAD1
301 for ubiquitination and degradation in transfected HEK293T cells (Guan et al., 2022). Loss of TRIP13
302 leads to accumulation of HORMAD proteins only to the synapsed SC in pachytene cells. In contrast,
303 depletion of SKP1 causes accumulation of HORMA domain proteins, particularly HORMAD1, on both
304 unsynapsed and synapsed chromosome axes from leptotene through diplotene meiocytes. Therefore,
305 TRIP13 and SKP1 might regulate different pools of HORMAD proteins in meiocytes.
306 In many organisms including mouse and human, centromeres are the last regions to synapse (Bisig
307 et al., 2012; Brown et al., 2005; Qiao et al., 2012). The reason for this is unknown, but it might be related
308 to the necessity to suppress deleterious non-homologous recombination at centromere and pericentromeric

309 regions, which consist of minor and major satellite repeats respectively. The centromere was proposed to
310 exert an inhibitory effect on synapsis in human cells (Brown et al., 2005). The inhibition needs to be
311 relieved to achieve full synapsis, since unsynapsis at centromeres is expected to trigger the meiotic
312 checkpoint, leading to meiotic arrest. To date, only two mouse mutants (*Skp1* and *Trip13*) exhibit
313 unsynapsis preferentially at the centromeric end in pachytene-like cells. In addition, only these two mouse
314 mutants display abnormal accumulation of HORMAD proteins on the synapsed SC. Intriguingly, TRIP13
315 localizes to telomeres in both spermatocytes and oocytes. The centromere is close to one of the telomeres
316 in mouse. Thus, the preferential centromeric end asynapsis in *Trip13* or *Skp1*-deficient meiocytes could be
317 related to abnormal persistence of HORMAD proteins. However, the underlying molecular mechanism
318 warrants further investigation.
319 We find that TRIP13 is a dosage-dependent regulator of meiosis. The *Trip13*$^{+/-}$ mice displayed
320 reduced testis weight, reduced sperm count, and meiotic defects but these defects were less severe than
321 the *Trip13*$^{-/-}$ mice. The disease phenotypes in humans also appear to be influenced by the *TRIP13* dosage
322 (Yost et al., 2017; Zhang et al., 2020). The dosage-dependent phenotypic variation has been reported in
323 other mouse meiotic mutants such as *Tex11*, *Meiob*, and *Rnf212*. TEX11 localizes to meiotic
324 chromosomes as foci and regulates crossover formation and chromosome synapsis (Yang et al., 2008).
325 The TEX11 protein levels correlate with genome-wide recombination rates in mice (Yang et al., 2015).
326 MEIOB, a meiosis-specific ssDNA-binding protein, is essential for meiotic recombination (Luo et al.,
327 2013; Souquet et al., 2013). In mice with different combinations of *Meiob* alleles, MEIOB protein levels
328 directly correlate with the severity of meiotic defects (Guo et al., 2020). Sequence variants in human
329 RNF212 are associated with variations in genome-wide recombination rates (Chowdhury et al., 2009;
330 Kong et al., 2008). In mouse, RNF212 forms foci on meiotic chromosomes and regulates crossover
331 formation in a dosage-dependent manner (Reynolds et al., 2013). Therefore, dosage sensitivity appears to
332 be a common feature of many regulators of meiosis.
333
334 **Materials and Methods**
335
336 **Ethics statement**
337 Mice were maintained and used for experimentation according to the protocol approved by the
338 Institutional Care and Use Committee of the University of Pennsylvania.
339
340 **Mouse strains**

341 The cryopreserved sperm from *Trip13*$^{+/-}$ males were obtained from the Mutant Mouse Resource and
342 Research Center (MMRCC) at UC Davis (*Trip13*$^{tm1.1(KOMP)Vlcg/JMmucd}$, MMRRC_050223-UCD).
343 Genotyping of wild type and knockout *Trip13* alleles was performed by separate PCR reactions using tail
344 genomic DNA. Other mutant mouse lines used in this study were previously generated: *Hormad1*, *Sycp2*,
345 and *Rec8* (Guan et al., 2020; Shin et al., 2010; Yang et al., 2006). Genotyping PCR primer sequences are
346 listed in Table 2.
347

348 **Generation of 3×FLAG-*Trip13* and *Trip13*-3×FLAG knockin mouse strains**

349 The 3×FLAG-knockin mouse strains were generated by the CRISPR-Cas9 mediated genome editing
350 approach. To generate N-terminally tagged knockin mice, one single-guide RNA (sgRNA) was designed
351 to target the first exon of the mouse *Trip13* (Figure 7 – figure supplement 1A). A ssDNA repair template
352 was created using the sequence surrounding the start codon as 5′ and 3′ homology arms. The knockin
353 template itself included the sequence for the 3×FLAG epitope and a three-residue linker sequence. The C-
354 terminally tagged strain was generated similarly (Figure 7 – figure supplement 1B). The guide RNA
355 targeted exon 13 containing the stop codon. The ssDNA template contained the FLAG-encoding
356 sequences and homology sequences flanking the insertion site. sgRNA sequences and ssDNA template
357 sequences were shown in Table 2.
358 For the sgRNA, the oligo was phosphorylated, annealed, and cloned to PX330 plasmid (Addgene,
359 Waterton, MA). After *in vitro* transcription with the MEGAshortscript T7 Kit (AM1354, Invitrogen) and
360 purification with the MEGAclear Transcription Clean-Up Kit (AM1908, Invitrogen), a mixture of Cas9
361 mRNA [100ng/µl; Trilink, catalog number L-7206) + 0.5 µl of the sgRNA (35 ng/µl) + 100ng/ul of
362 ssDNA template] was prepared and injected into zygotes. The injected zygotes were cultured in KSOM
363 medium at 37°C in a 5% CO_2 incubator until the two-cell stage. The two-cell embryos were transferred
364 into oviducts of 0.5-day post-coitum pseudopregnant ICR foster mothers. Founder mice were bred to wild
365 type mice to obtain germline transmission. The N-terminal 3×FLAG allele and the C-terminal 3×FLAG
366 allele were PCR amplified and sequenced to confirm the insertion. PCR genotyping primers are listed in
367 Table 2.
368

369 **Production of anti-MAJIN antibodies**

370 The short isoform of mouse MAJIN (amino acids 1-124; XM_036161650.1 and XP_036017543.1) was
371 expressed as a 6xHis-MAJIN recombinant protein in *E. coli* using the pQE-30 vector. The recombinant
372 protein was affinity purified with the Ni-NTA agarose. Two guinea pigs were immunized at Cocalico

373 Biologicals Inc. (Reamstown, PA), resulting in two antisera (UP-GP140 and UP-GP141). Both anti-sera
374 were used for immunofluorescence of nuclear spreads of spermatocytes.
375
376 **Histological, immunofluorescence, and surface nuclear spread analyses**
377 For histology, testes or ovaries were fixed in Bouin's solution at room temperature overnight, embedded
378 with paraffin, and sectioned at 8 μm. Sections were stained with hematoxylin and eosin. For
379 immunofluorescence analysis, testes were fixed in 4% paraformaldehyde (in 1×PBS) overnight at 4°C,
380 dehydrated in 30% sucrose (in 1×PBS) overnight, and sectioned at 8 μm in a cryostat. Surface nuclear
381 spread analysis was described before (Peters et al., 1997). Briefly, testicular tubules or ovarian tissues
382 were soaked in hypotonic treatment buffer (30 mM Tris, 50 mM sucrose, 17 mM trisodium citrate
383 dihydrate, 5 mM EDTA, 0.5 mM DTT, 1 mM PMSF). Then the cells were suspended in 100 mM sucrose
384 and spread by physical disruption on "PTFE" printed slides that were previously soaked with
385 paraformaldehyde solution containing Triton X-100 and sodium borate. Antibodies used for
386 immunostaining are listed in Table 3.
387
388 **Imaging**
389 Histological images were captured on the Leica DM5500B microscope with a DFC450 digital camera
390 (Leica Microsystems, Wetzlar, Germany). Most immunolabeled chromosome spread images were taken
391 on the Leica DM5500B microscope with an ORCA Flash4.0 digital monochrome camera (Hamamatsu
392 Photonics, Bridgewater, NJ). Confocal microscopy of immunolabeled chromosome spreads was
393 performed on a Leica SP5 II confocal (Leica Microsystems, Wetzlar, Germany) with an 100× (1.46 NA)
394 oil immersion objective lens. Images were deconvolved with Huygens Essential deconvolution software
395 (Scientific Volume Imaging B.V., Hilversum, Netherlands).
396
397 ***Western blot analysis***
398 Testes were homogenized in the lysis buffer (50 mM Tris-HCl, pH 8.0, 150 mM NaCl, 1% Trion X-100,
399 0.5% sodium deoxycholate, 5 mM $MgCl_2$, and 1 mM DTT supplemented with 1 mM PMSF). 40 μg of
400 protein samples were resolved by SDS-PAGE, transferred onto PDVF membranes, and immunoblotted
401 with primary antibodies (Table 3).
402
403 **Acknowledgements**
404 We thank Gordon Ruthel at the PennVet Imaging Core for help with super-resolution microscopy, Hsin
405 Yao Tang and Thomas Beer at Wistar Proteomics Core for help with mass spectrometry, Christer Hoog

for SYCP1 antibody, Attila Toth for HORMAD2 antibody, Yoshinori Watanabe and Takashi Akera for CENP-C antibody.

Competing interests: The authors declare that no competing interests exist.

Funding

This work was supported by National Institutes of Health/National Institute of Child Health and Human Development grants T32HD083185 (JYC), R01HD069592 (PJW), and P50HD068157 (PJW).

References

Balboni, M., Yang, C., Komaki, S., Brun, J. and Schnittger, A. (2020). COMET Functions as a PCH2 Cofactor in Regulating the HORMA Domain Protein ASY1. *Curr Biol* 30, 4113-4127 e4116.

Bisig, C. G., Guiraldelli, M. F., Kouznetsova, A., Scherthan, H., Hoog, C., Dawson, D. S. and Pezza, R. J. (2012). Synaptonemal complex components persist at centromeres and are required for homologous centromere pairing in mouse spermatocytes. *PLoS genetics* 8, e1002701.

Brown, P. W., Judis, L., Chan, E. R., Schwartz, S., Seftel, A., Thomas, A. and Hassold, T. J. (2005). Meiotic synapsis proceeds from a limited number of subtelomeric sites in the human male. *American Journal of Human Genetics* 77, 556-566.

Chen, C., Jomaa, A., Ortega, J. and Alani, E. E. (2014). Pch2 is a hexameric ring ATPase that remodels the chromosome axis protein Hop1. *Proceedings of the National Academy of Sciences of the United States of America* 111, 44.

Chowdhury, R., Bois, P. R., Feingold, E., Sherman, S. L. and Cheung, V. G. (2009). Genetic analysis of variation in human meiotic recombination. *PLoS genetics* 5, e1000648.

Daniel, K., Lange, J., Hached, K., Fu, J., Anastassiadis, K., Roig, I., Cooke, H. J., Stewart, A. F., Wassmann, K., Jasin, M., et al. (2011). Meiotic homologue alignment and its quality surveillance are controlled by mouse HORMAD1. *Nature cell biology* 13, 599-610.

de Vries, F. A., de Boer, E., van den Bosch, M., Baarends, W. M., Ooms, M., Yuan, L., Liu, J. G., van Zeeland, A. A., Heyting, C. and Pastink, A. (2005). Mouse Sycp1 functions in synaptonemal complex assembly, meiotic recombination, and XY body formation. *Genes & development* 19, 1376-1389.

Deshong, A. J., Ye, A. L., Lamelza, P. and Bhalla, N. (2014). A quality control mechanism coordinates meiotic prophase events to promote crossover assurance. *PLoS Genet* 10, e1004291.

Fukuda, T., Daniel, K., Wojtasz, L., Toth, A. and Hoog, C. (2010). A novel mammalian HORMA domain-containing protein, HORMAD1, preferentially associates with unsynapsed meiotic chromosomes. *Experimental cell research* 316, 158-171.

Gomez, H. L., Felipe-Medina, N., Condezo, Y. B., Garcia-Valiente, R., Ramos, I., Suja, J. A., Barbero, J. L., Roig, I., Sanchez-Martin, M., de Rooij, D. G., et al. (2019). The PSMA8 subunit of the spermatoproteasome is essential for proper meiotic exit and mouse fertility. *PLoS Genet* 15, e1008316.

Guan, Y., Leu, N. A., Ma, J., Chmatal, L., Ruthel, G., Bloom, J. C., Lampson, M. A., Schimenti, J. C., Luo, M. and Wang, P. J. (2020). SKP1 drives the prophase I to metaphase I transition during male meiosis. *Science advances* 6, eaaz2129.

Guan, Y., Lin, H., Leu, N. A., Ruthel, G., Fuchs, S. Y., Busino, L., Luo, M. and Wang, P. J. (2022). SCF ubiquitin E3 ligase regulates DNA double-strand breaks in early meiotic recombination. *Nucleic Acids Res* 50, 5129-5144.

449 Guo, R., Xu, Y., Leu, N. A., Zhang, L., Fuchs, S. Y., Ye, L. and Wang, P. J. (2020). The ssDNA-binding
450 protein MEIOB acts as a dosage-sensitive regulator of meiotic recombination. *Nucleic acids research*
451 48, 12219-12233.
452 Handel, M. A. and Schimenti, J. C. (2010). Genetics of mammalian meiosis: regulation, dynamics and
453 impact on fertility. *Nature reviews.Genetics* 11, 124-136.
454 Herruzo, E., Lago-Maciel, A., Baztan, S., Santos, B., Carballo, J. A. and San-Segundo, P. A. (2021). Pch2
455 orchestrates the meiotic recombination checkpoint from the cytoplasm. *PLoS Genet* 17, e1009560.
456 Herruzo, E., Ontoso, D., Gonzalez-Arranz, S., Cavero, S., Lechuga, A. and San-Segundo, P. A. (2016).
457 The Pch2 AAA+ ATPase promotes phosphorylation of the Hop1 meiotic checkpoint adaptor in
458 response to synaptonemal complex defects. *Nucleic Acids Res* 44, 7722-7741.
459 Hunter, N. (2015). Meiotic Recombination: The Essence of Heredity. *Cold Spring Harbor perspectives in*
460 *biology* 7, 10.1101/cshperspect.a016618.
461 Joshi, N., Barot, A., Jamison, C. and Borner, G. V. (2009). Pch2 links chromosome axis remodeling at
462 future crossover sites and crossover distribution during yeast meiosis. *PLoS Genet* 5, e1000557.
463 Karlseder, J., Kachatrian, L., Takai, H., Mercer, K., Hingorani, S., Jacks, T. and de Lange, T. (2003).
464 Targeted deletion reveals an essential function for the telomere length regulator Trf1. *Molecular and*
465 *cellular biology* 23, 6533-6541.
466 Kim, J., Ishiguro, K., Nambu, A., Akiyoshi, B., Yokobayashi, S., Kagami, A., Ishiguro, T., Pendas, A. M.,
467 Takeda, N., Sakakibara, Y., et al. (2015). Meikin is a conserved regulator of meiosis-I-specific
468 kinetochore function. *Nature* 517, 466-471.
469 Kim, Y., Rosenberg, S. C., Kugel, C. L., Kostow, N., Rog, O., Davydov, V., Su, T. Y., Dernburg, A. F.
470 and Corbett, K. D. (2014). The chromosome axis controls meiotic events through a hierarchical
471 assembly of HORMA domain proteins. *Dev Cell* 31, 487-502.
472 Klare, K., Weir, J. R., Basilico, F., Zimniak, T., Massimiliano, L., Ludwigs, N., Herzog, F. and
473 Musacchio, A. (2015). CENP-C is a blueprint for constitutive centromere-associated network assembly
474 within human kinetochores. *The Journal of cell biology* 210, 11-22.
475 Kogo, H., Tsutsumi, M., Inagaki, H., Ohye, T., Kiyonari, H. and Kurahashi, H. (2012a). HORMAD2 is
476 essential for synapsis surveillance during meiotic prophase via the recruitment of ATR activity. *Genes*
477 *Cells* 17, 897-912.
478 Kogo, H., Tsutsumi, M., Ohye, T., Inagaki, H., Abe, T. and Kurahashi, H. (2012b). HORMAD1-
479 dependent checkpoint/surveillance mechanism eliminates asynaptic oocytes. *Genes Cells* 17, 439-454.
480 Kong, A., Thorleifsson, G., Stefansson, H., Masson, G., Helgason, A., Gudbjartsson, D. F., Jonsdottir, G.
481 M., Gudjonsson, S. A., Sverrisson, S., Thorlacius, T., et al. (2008). Sequence variants in the RNF212
482 gene associate with genome-wide recombination rate. *Science (New York, N.Y.)* 319, 1398-1401.
483 Kwon, M. S., Hori, T., Okada, M. and Fukagawa, T. (2007). CENP-C is involved in chromosome
484 segregation, mitotic checkpoint function, and kinetochore assembly. *Mol Biol Cell* 18, 2155-2168.
485 Lambing, C., Osman, K., Nuntasoontorn, K., West, A., Higgins, J. D., Copenhaver, G. P., Yang, J.,
486 Armstrong, S. J., Mechtler, K., Roitinger, E., et al. (2015). Arabidopsis PCH2 Mediates Meiotic
487 Chromosome Remodeling and Maturation of Crossovers. *PLoS Genet* 11, e1005372.
488 Li, X. C. and Schimenti, J. C. (2007). Mouse pachytene checkpoint 2 (trip13) is required for completing
489 meiotic recombination but not synapsis. *PLoS genetics* 3, e130.
490 Long, J., Huang, C., Chen, Y., Zhang, Y., Shi, S., Wu, L., Liu, Y., Liu, C., Wu, J. and Lei, M. (2017).
491 Telomeric TERB1-TRF1 interaction is crucial for male meiosis. *Nat Struct Mol Biol* 24, 1073-1080.
492 Luo, M., Yang, F., Leu, N. A., Landaiche, J., Handel, M. A., Benavente, R., La Salle, S. and Wang, P. J.
493 (2013). MEIOB exhibits single-stranded DNA-binding and exonuclease activities and is essential for
494 meiotic recombination. *Nature communications* 4, 2788.
495 Luo, X., Tang, Z., Xia, G., Wassmann, K., Matsumoto, T., Rizo, J. and Yu, H. (2004). The Mad2 spindle
496 checkpoint protein has two distinct natively folded states. *Nat Struct Mol Biol* 11, 338-345.

497 Miao, C., Tang, D., Zhang, H., Wang, M., Li, Y., Tang, S., Yu, H., Gu, M. and Cheng, Z. (2013). Central
498 region component1, a novel synaptonemal complex component, is essential for meiotic recombination
499 initiation in rice. *Plant Cell* 25, 2998-3009.
500 Pacheco, S., Marcet-Ortega, M., Lange, J., Jasin, M., Keeney, S. and Roig, I. (2015). The ATM signaling
501 cascade promotes recombination-dependent pachytene arrest in mouse spermatocytes. *PLoS genetics*
502 11, e1005017.
503 Page, S. L. and Hawley, R. S. (2004). The genetics and molecular biology of the synaptonemal complex.
504 *Annual Review of Cell and Developmental Biology* 20, 525-558.
505 Peters, A. H., Plug, A. W., van Vugt, M. J. and de Boer, P. (1997). A drying-down technique for the
506 spreading of mammalian meiocytes from the male and female germline. *Chromosome research : an*
507 *international journal on the molecular, supramolecular and evolutionary aspects of chromosome*
508 *biology* 5, 66-68.
509 Prince, J. P. and Martinez-Perez, E. (2022). Functions and Regulation of Meiotic HORMA-Domain
510 Proteins. *Genes (Basel)* 13.
511 Qiao, H., Chen, J. K., Reynolds, A., Hoog, C., Paddy, M. and Hunter, N. (2012). Interplay between
512 synaptonemal complex, homologous recombination, and centromeres during mammalian meiosis.
513 *PLoS genetics* 8, e1002790.
514 Raina, V. B. and Vader, G. (2020). Homeostatic Control of Meiotic Prophase Checkpoint Function by
515 Pch2 and Hop1. *Curr Biol* 30, 4413-4424 e4415.
516 Reynolds, A., Qiao, H., Yang, Y., Chen, J. K., Jackson, N., Biswas, K., Holloway, J. K., Baudat, F., de
517 Massy, B., Wang, J., et al. (2013). RNF212 is a dosage-sensitive regulator of crossing-over during
518 mammalian meiosis. *Nature genetics* 45, 269-278.
519 Rinaldi, V. D., Bolcun-Filas, E., Kogo, H., Kurahashi, H. and Schimenti, J. C. (2017). The DNA Damage
520 Checkpoint Eliminates Mouse Oocytes with Chromosome Synapsis Failure. *Mol Cell* 67, 1026-1036
521 e1022.
522 Roeder, G. S. and Bailis, J. M. (2000). The pachytene checkpoint. *Trends in genetics : TIG; Trends in*
523 *genetics : TIG* 16, 395-403.
524 Roig, I., Dowdle, J. A., Toth, A., de Rooij, D. G., Jasin, M. and Keeney, S. (2010). Mouse TRIP13/PCH2
525 is required for recombination and normal higher-order chromosome structure during meiosis. *PLoS*
526 *genetics* 6, 10.1371/journal.pgen.1001062.
527 Russo, A. E., Giacopazzi, S., Deshong, A., Menon, M., Ortiz, V., Ego, K. M., Corbett, K. D. and Bhalla,
528 N. (2023). The conserved AAA ATPase PCH-2 distributes its regulation of meiotic prophase events
529 through multiple meiotic HORMADs in C. elegans. *PLoS Genet* 19, e1010708.
530 San-Segundo, P. A. and Roeder, G. S. (1999). Pch2 links chromatin silencing to meiotic checkpoint
531 control. *Cell* 97, 313-324.
532 Shibuya, H., Hernandez-Hernandez, A., Morimoto, A., Negishi, L., Hoog, C. and Watanabe, Y. (2015).
533 MAJIN Links Telomeric DNA to the Nuclear Membrane by Exchanging Telomere Cap. *Cell* 163,
534 1252-1266.
535 Shibuya, H., Ishiguro, K. and Watanabe, Y. (2014). The TRF1-binding protein TERB1 promotes
536 chromosome movement and telomere rigidity in meiosis. *Nature cell biology* 16, 145-156.
537 Shin, Y. H., Choi, Y., Erdin, S. U., Yatsenko, S. A., Kloc, M., Yang, F., Wang, P. J., Meistrich, M. L. and
538 Rajkovic, A. (2010). Hormad1 mutation disrupts synaptonemal complex formation, recombination, and
539 chromosome segregation in mammalian meiosis. *PLoS genetics* 6, e1001190.
540 Sironi, L., Mapelli, M., Knapp, S., De Antoni, A., Jeang, K. T. and Musacchio, A. (2002). Crystal
541 structure of the tetrameric Mad1-Mad2 core complex: implications of a 'safety belt' binding mechanism
542 for the spindle checkpoint. *EMBO J* 21, 2496-2506.
543 Souquet, B., Abby, E., Herve, R., Finsterbusch, F., Tourpin, S., Le Bouffant, R., Duquenne, C., Messiaen,
544 S., Martini, E., Bernardino-Sgherri, J., et al. (2013). MEIOB Targets Single-Strand DNA and Is
545 Necessary for Meiotic Recombination. *PLoS genetics* 9, e1003784.

546 Stanzione, M., Baumann, M., Papanikos, F., Dereli, I., Lange, J., Ramlal, A., Trankner, D., Shibuya, H.,
547 de Massy, B., Watanabe, Y., et al. (2016). Meiotic DNA break formation requires the unsynapsed
548 chromosome axis-binding protein IHO1 (CCDC36) in mice. *Nature cell biology* 18, 1208-1220.
549 Subramanian, V. V., MacQueen, A. J., Vader, G., Shinohara, M., Sanchez, A., Borde, V., Shinohara, A.
550 and Hochwagen, A. (2016). Chromosome Synapsis Alleviates Mek1-Dependent Suppression of
551 Meiotic DNA Repair. *PLoS Biol* 14, e1002369.
552 West, A. M., Rosenberg, S. C., Ur, S. N., Lehmer, M. K., Ye, Q., Hagemann, G., Caballero, I., Uson, I.,
553 MacQueen, A. J., Herzog, F., et al. (2019). A conserved filamentous assembly underlies the structure
554 of the meiotic chromosome axis. *Elife* 8.
555 West, A. M. V., Komives, E. A. and Corbett, K. D. (2018). Conformational dynamics of the Hop1
556 HORMA domain reveal a common mechanism with the spindle checkpoint protein Mad2. *Nucleic*
557 *Acids Res* 46, 279-292.
558 Wojtasz, L., Cloutier, J. M., Baumann, M., Daniel, K., Varga, J., Fu, J., Anastassiadis, K., Stewart, A. F.,
559 Reményi, A., Turner, J. M., et al. (2012). Meiotic DNA double-strand breaks and chromosome
560 asynapsis in mice are monitored by distinct HORMAD2-independent and -dependent mechanisms.
561 *Genes Dev* 26, 958-973.
562 Wojtasz, L., Daniel, K., Roig, I., Bolcun-Filas, E., Xu, H., Boonsanay, V., Eckmann, C. R., Cooke, H. J.,
563 Jasin, M., Keeney, S., et al. (2009). Mouse HORMAD1 and HORMAD2, two conserved meiotic
564 chromosomal proteins, are depleted from synapsed chromosome axes with the help of TRIP13 AAA-
565 ATPase. *PLoS genetics* 5, e1000702.
566 Xu, H., Beasley, M. D., Warren, W. D., van der Horst, G. T. and McKay, M. J. (2005). Absence of mouse
567 REC8 cohesin promotes synapsis of sister chromatids in meiosis. *Developmental cell* 8, 949-961.
568 Xu, H., Tong, Z., Ye, Q., Sun, T., Hong, Z., Zhang, L., Bortnick, A., Cho, S., Beuzer, P., Axelrod, J., et
569 al. (2019). Molecular organization of mammalian meiotic chromosome axis revealed by expansion
570 STORM microscopy. *Proc Natl Acad Sci U S A* 116, 18423-18428.
571 Yang, C., Hu, B., Portheine, S. M., Chuenban, P. and Schnittger, A. (2020). State changes of the HORMA
572 protein ASY1 are mediated by an interplay between its closure motif and PCH2. *Nucleic Acids Res* 48,
573 11521-11535.
574 Yang, C., Sofroni, K., Hamamura, Y., Hu, B., Elbasi, H. T., Balboni, M., Chu, L., Stang, D., Heese, M.
575 and Schnittger, A. (2022). ZYP1-mediated recruitment of PCH2 to the synaptonemal complex
576 remodels the chromosome axis leading to crossover restriction. *Nucleic Acids Res* 50, 12924-12937.
577 Yang, F., De La Fuente, R., Leu, N. A., Baumann, C., McLaughlin, K. J. and Wang, P. J. (2006). Mouse
578 SYCP2 is required for synaptonemal complex assembly and chromosomal synapsis during male
579 meiosis. *The Journal of cell biology* 173, 497-507.
580 Yang, F., Gell, K., van der Heijden, G. W., Eckardt, S., Leu, N. A., Page, D. C., Benavente, R., Her, C.,
581 Hoog, C., McLaughlin, K. J., et al. (2008). Meiotic failure in male mice lacking an X-linked factor.
582 *Genes & development* 22, 682-691.
583 Yang, F., Silber, S., Leu, N. A., Oates, R. D., Marszalek, J. D., Skaletsky, H., Brown, L. G., Rozen, S.,
584 Page, D. C. and Wang, P. J. (2015). TEX11 is mutated in infertile men with azoospermia and regulates
585 genome-wide recombination rates in mouse. *EMBO molecular medicine* 7, 1198-1210.
586 Ye, Q., Kim, D. H., Dereli, I., Rosenberg, S. C., Hagemann, G., Herzog, F., Toth, A., Cleveland, D. W.
587 and Corbett, K. D. (2017). The AAA+ ATPase TRIP13 remodels HORMA domains through N-
588 terminal engagement and unfolding. *EMBO J* 36, 2419-2434.
589 Yost, S., de Wolf, B., Hanks, S., Zachariou, A., Marcozzi, C., Clarke, M., de Voer, R., Etemad, B.,
590 Uijttewaal, E., Ramsay, E., et al. (2017). Biallelic TRIP13 mutations predispose to Wilms tumor and
591 chromosome missegregation. *Nat Genet* 49, 1148-1151.
592 Zhang, Z., Li, B., Fu, J., Li, R., Diao, F., Li, C., Chen, B., Du, J., Zhou, Z., Mu, J., et al. (2020). Bi-allelic
593 Missense Pathogenic Variants in TRIP13 Cause Female Infertility Characterized by Oocyte Maturation
594 Arrest. *American Journal of Human Genetics* 107, 15-23.

595 Zickler, D. and Kleckner, N. (2015). Recombination, Pairing, and Synapsis of Homologs during Meiosis.
596 *Cold Spring Harbor perspectives in biology* 7, 10.1101/cshperspect.a016626.
597

598

599 **Figure Legends**

600

601 **Figure 1.** TRIP13 localizes to the synaptonemal complex and telomeres in spermatocytes. (A) Western
602 blot analysis of TRIP13 in adult mouse tissues. Heart and skeletal muscle lack ACTB. (B)
603 Immunofluorescence of TRIP13 in sections of 3-month-old wild type and *Trip13*$^{-/-}$ testes. Lep, leptotene;
604 Zyg, zygotene; Dip, diplotene; eS, elongating spermatids; ES, elongated spermatids. (C)
605 Immunofluorescence of TRIP13 in spread nuclei of spermatocytes from wild type P20 testes. (D) Super-
606 resolution localization of TRIP13 to the central element (CE) but not lateral element (LE) of the
607 synaptonemal complex at early pachytene stage. The enlarged view of the boxed chromosome is shown at
608 the bottom.

609

610 **Figure 2.** Loss of *Trip13* leads to meiotic arrest in males. (A) Image of testes from 2 to 3 month-old mice.
611 (B) Western blot analysis of TRIP13 in P21 testes. SYCP3 serves as a meiosis-specific marker. ACTB
612 serves as a loading control. (C) Testis to body weight ratio of 2 to 3 month-old mice. n = 3 males.
613 Statistics, one-Way ANOVA. (D) Sperm count of 2 to 3 month-old *Trip13*$^{+/+}$ and *Trip13*$^{+/-}$ males. n = 3
614 males. Statistics, one-Way ANOVA. (E) Histological analysis of 2-month-old testes. Sertoli, Sertoli cell;
615 Zyg, zygotene; Pa-like, pachytene-like; Dip, diplotene; eS, elongating spermatids.

616

617 **Figure 3.** *Trip13* is required for chromosomal synapsis in males. (A) Composition of prophase I
618 spermatocytes in P20 testes. Three males per genotype were analyzed by nuclear spread analysis. Total
619 number of spermatocytes counted: *Trip13*$^{+/+}$, 1038 cells; *Trip13*$^{+/-}$, 803 cells; *Trip13*$^{-/-}$, 406 cells. (B)
620 Immunofluorescence of SYCP1 and SYCP3 in spread nuclei of pachytene spermatocytes from P20 testes.
621 (C) Immunofluorescence of SYCE1 and SYCP3 in spread nuclei of pachytene spermatocytes from P20
622 testes. (D) Super-resolution confocal microscopy of a *Trip13*$^{-/-}$ spermatocyte from P20 testis.
623 Immunostaining was performed for SYCP1 and SYCP3. Arrowheads indicate end asynapsis. Arrow
624 indicates interstitial asynapsis. (E) Percentage of early pachytene cells from P19-20 testes with asynapsed
625 chromosomes across three genotypes. (F) Number of homologous chromosomes with end asynapsis per
626 cell in P19-20 testes. (G) Percentage of early pachytene cells from P20 testes with asynapsed XY
627 chromosomes per mouse. The *p* values are indicated in graphs. Statistics (E-G), one-way ANOVA.

628

629 **Figure 4.** Normal localization of centromere and telomere markers in *Trip13*-deficient spermatocytes
630 from juvenile mice. (A-D) Immunofluorescent analysis of centromere and telomere markers in *Trip13*$^{+/+}$

631 and *Trip13*$^{-/-}$ pachytene spermatocytes: CREST (A), CENPC (B), TRF1 (C), and MAJIN (D). SYCP3
632 labels the lateral elements of the synaptonemal complex. Scale bars, 10 µm.
633
634 **Figure 5.** HORMAD1 and HORMAD2 accumulate on the lateral elements of synapsed autosomes in
635 *Trip13*$^{-/-}$ spermatocytes from juvenile (P19-21) mice. (A, B) Immunofluorescence of HORMAD1 (A) and
636 HORMAD2 (B) in pachytene spermatocytes. (C, D) Super-resolution imaging of HORMAD1 and
637 HORMAD2 in zygotene and pachytene spermatocytes. Enlarged views of the boxed chromosomes are
638 shown below. Scale bars: 10 µm (A, B), 5 µm (C, D).
639
640 **Figure 6.** Localization of TRIP13 to the SC is independent of individual axial element components. (A)
641 Immunofluorescent analysis of TRIP13 in *Hormad1*$^{-/-}$ spermatocytes from 2-month-old mice. (B)
642 Immunofluorescent analysis of TRIP13 in *Rec8*$^{-/-}$ spermatocytes from 2-month -old mice. (C)
643 Immunofluorescent analysis of TRIP13 in *Sycp2*$^{-/-}$ spermatocytes from 2-month -old mice. (D)
644 Immunofluorescent analysis of TRIP13 in *Skp1*^{cKO} spermatocytes from 2-month -old mice. Scale bars, 10
645 µm.
646
647 **Figure 7.** FLAG-tagged TRIP13 proteins localize correctly and are functional. (A) Western blot analysis
648 of tagged and untagged TRIP13 proteins in testes from P20 wild type (no tag), heterozygous tagged, and
649 homozygous tagged males. (D) Immunofluorescence of FLAG-tagged TRIP13 in pachytene
650 spermatocytes from P20 homozygous testes. N-terminal tag, 3×FLAG-*Trip13*; C-terminal tag, *Trip13*-
651 3×FLAG. Scale bar, 10 µm.
652
653 **Figure 1 - figure supplement 1.** Immunofluorescent analysis of TRIP13 in spread nuclei of oocytes from
654 embryonic day 16.5 (E16.5) and E18.5 female embryos. Scale bars, 10 µm.
655
656 **Figure 2 - figure supplement 1.** Histological analysis of ovaries from adult (8-week) wild type and
657 *Trip13*$^{-/-}$ females. Scale bars, 200 µm.
658
659 **Figure 7 - figure supplement 1.** Generation of two *Trip13* FLAG tagged mouse lines. (A) Illustration of
660 the *Trip13* gene structure with the 3×FLAG tag at the N terminus. The guide RNA sequence is underlined
661 in green. The single strand DNA (ssDNA) oligo template (200 nt) contains the 3×FLAG-encoding
662 sequence. The PAM site is underlined in purple. One base in the PAM site is mutated in the ssDNA oligo
663 template to prevent cutting of the template strand (in purple). The position of 3×FLAG in-frame insertion

664 is designated (^) and occurs just after the endogenous start codon. Filled bars, coding regions; Open bars,
665 5′ or 3′ UTRs. (B) Illustration of the *Trip13* gene structure with the 3×FLAG tag at the C terminus. The
666 PAM cut site and guide RNA were on the reverse strand, but for clarity, the forward strand sequence is
667 shown. The 3×FLAG was inserted just before the endogenous stop codon.
668
669

670
671
672
673 **Table 1**. **List of proteins from testis identified by co-immunoprecipitation and mass spectrometry**.
674

Protein	Number of peptides in anti-FLAG IP			M.W. (kD)
	3×FLAG-TRIP13 testis	TRIP13-3×FLAG testis	Wild type testis	
TRIP13	28	36	4	51
HORMAD2	21	10	7	39
DDX46	32	6	0	117
PUF60	24	14	0	59
RBM25	19	3	2	100
RBM39	20	10	1	59
U2AF1	11	4	1	28
U2AF2	15	9	3	54
SRSF11	9	4	0	53
SPATA5	26	27	7	97
AP3D1	17	6	2	135
PRPF40A	16	3	0	108
UGP2	15	3	0	57

675
676
677
678
679

680
681
682 **Table 2. Sequences of genotyping PCR primers, sgRNA, and ssDNA templates**

Genotyping primers			
Allele	Forward	Reverse	product (bp)
Trip13 WT	GCCCTTAGCCAAGGTGGAT	TCCTTGCACCCCTAATTGAC	645
Trip13 KO	ACTTGCTTTAAAAAACCTCCCACA	CAGAAAGCAACTGCTCCCTTCTAGC	731
Sycp2 WT	AGATGAGGGCATATCACCGA	TAAGCACACTCACCATCTCC	400
Sycp2 KO	GCATGTTATCAACCTTATCCCT	CCTACCGGTGGATGTGGAATGTGTG	300
Rec8 WT	AGCAGAGTCGAAGAAGGCCTCTTG	CAGATGGTGGCGAAGCAGCCTGT	426
Rec8 KO	AGCAGAGTCGAAGAAGGCCTCTTG	TTGCTCAGGGGAATTTGGGTC	212
Hormad1 WT	TCAAGACCAACCTGGGCTAC	CCATGTGGGTTGTAGGGAGT	196
Hormad1 KO	TCAAGACCAACCTGGGCTAC	GGGGAACTTCCTGACTAGGG	~400
3×FLAG-*Trip13*	CCTACATCGGAGAAGGCTGT	TTCATGTCAGGCTGTTCAGG	WT:348 KI:426
Trip13-3×FLAG	GCCCCACTAAAGCACAAGTC	ACAGGCTTGAGTCAGGATGG	WT:405 KI:471

Genome editing		
	guide RNA	HDR ssDNA
3×FLAG-*Trip13*	ATTCCCTCGGCTCCCGGCGG	TCGGAGAAGGCTGTCGCACAGGGCGCAGGGAGGCGA CCGCGGCCTCACTCCGGCGGCATTCCCTCGGCTCCCG GCGGCAGCGCCATGGGTGACTACAAAGACCATGACG GTGATTATAAAGATCATGACATCGATTACAAGGATGA CGATGACAAGGGAAGCGGAGACGAGGCGGTGGGCGA CCTGAAGCAAGCGCTTCC
Trip13-3×FLAG	AAGCCATAGATATGGATGTC	AGGGTTTCCTCCAGGCCCTATCTCTGGCAGTGGACAA ACAGTTTGAGGAGAAAAAGAAACTTTCAGCTTATGTT GACTACAAAGACCATGACGGTGATTATAAAGATCATG ACATCGATTACAAGGATGACGATGACAAGTGATCCAA GACATCCATATCTATGGCTTTCAATGGACAAGTAGGA GGTGATACCGTCTAC

683
684

685

686

687 **Table 3. List of primary antibodies**

Reagent	Dilution	Source	Catalog # or reference
Mouse anti-ACTB mab	1:2000	Sigma	Cat# A5441; RRID: AB_476744
Human anti-centromere (CREST)	1:500	Antibodies Incorporated	Cat# 15-234; RRID: AB_2687472
Rabbit anti-SYCP1	1:300	Abcam	Cat# ab15090; RRID: AB_301636
Guinea pig anti-SYCP2	1:150	Custom made	(Yang et al., 2006)
Mouse anti-SYCP3 mab	1:500	Abcam	Cat# ab97672; RRID: AB_10678841
Rabbit anti-SYCP3	1:500 IF; 1:2000 WB	ProteinTech Group	Cat# 23024-1-AP; RRID: AB_11232426
Rabbit anti-HORMAD1	1:300	ProteinTech Group	Cat# 13917-1-AP; RRID: AB_2120844
Rabbit anti-HORMAD2	1:500	Custom made, a gift from Toth lab	(Wojtasz et al., 2009)
Rabbit anti-REC8	1:200	Custom made, a gift ftom Mengcheng Luo lab	N/A
Mouse anti-FLAG mab	1:300IF; 1:4000WB	Sigma	Cat# F3165, RRID: AB_259529
Rabbit anti-SKP1	1:200 IF; 1:1000 WB	Cell Signaling	Cat# 12248S, RRID: AB_2754993
Rabbit anti-TRIP13	1:150 IF; 1:1000 WB	ProteinTech Group	19602-1-AP
Rabbit anti-SYCE1	1:200 IF; 1:1000 WB	Custom made	N/A
Mouse anti-SYCP1 mab	1:200 IF: 1:1000 WB	Custom made, 1:200; a gift from Chritster Hoog lab	N/A
Rabbit anti-CENP-C	1:500	Custom made, a gift from Y. Watanabe	(Kim et al., 2015)
Mouse anti-TRF1 mab	1:100	Sigma	T1948
Guinea pig anti- MAJIN	1:100	Custom made; this study	N/A

688

689

690

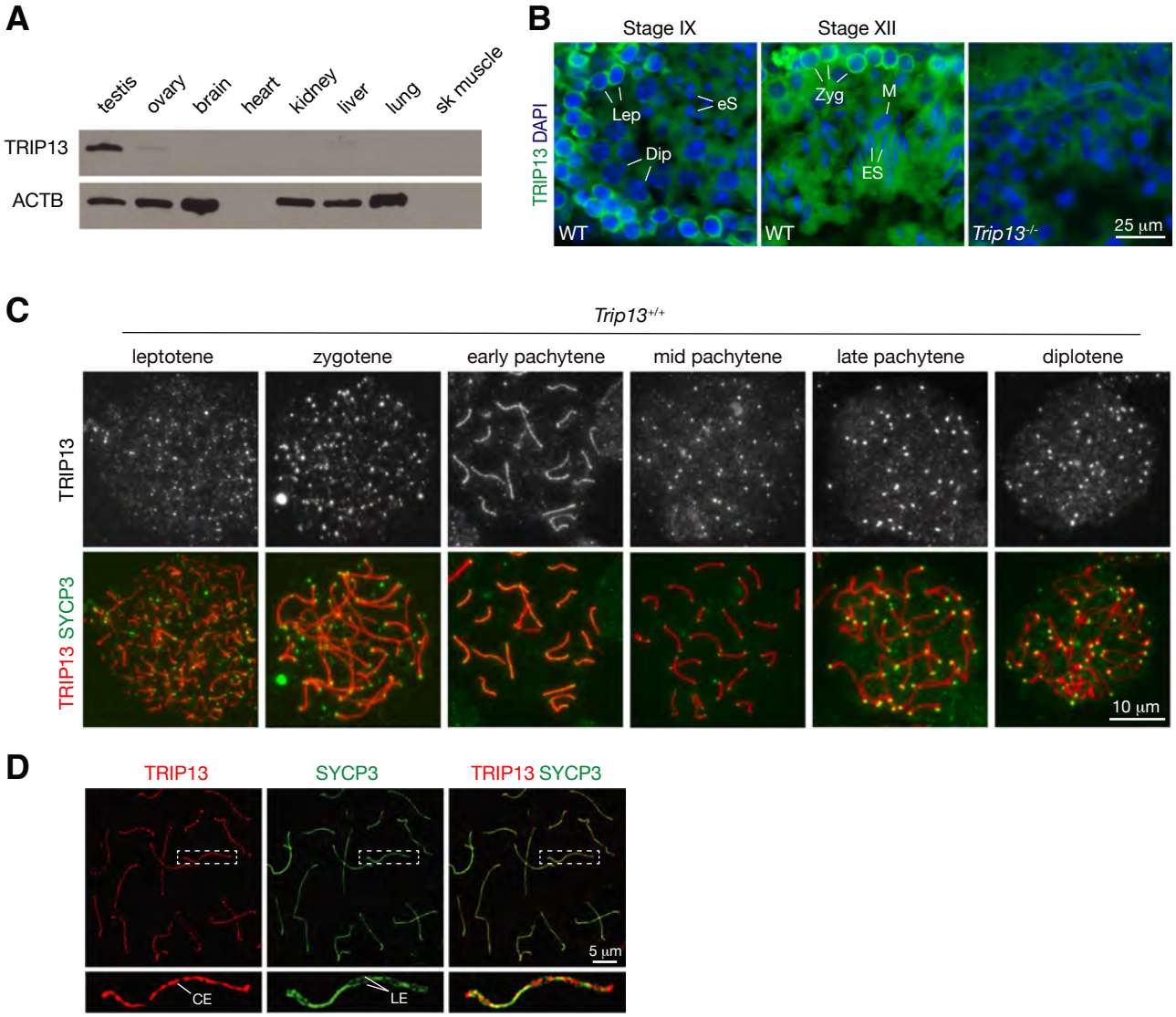
A
testis
ovary
brain
heart
kidney
liver
lung
sk muscle
TRIP13
ACTB
B
Stage IX
Stage XII
TRIP13 DAPI
Lep
eS
Dip
Zyg
M
ES
WT
WT
Trip13-/-
25 µm
C
Trip13+/+
leptotene
zygotene
early pachytene
mid pachytene
late pachytene
diplotene
TRIP13
TRIP13 SYCP3
10 µm
D
TRIP13
SYCP3
TRIP13 SYCP3
5 µm
CE
LE

Figure 1

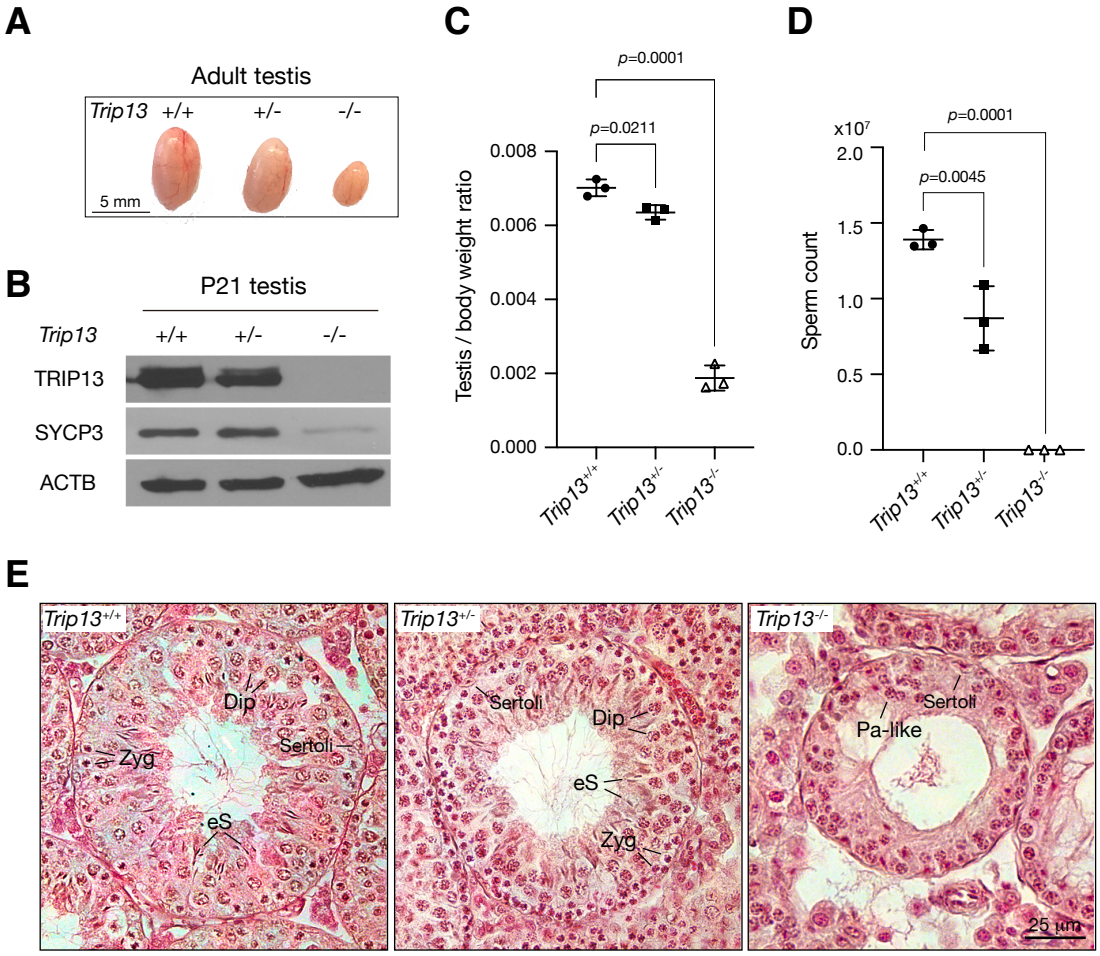
A
Adult testis
Trip13 +/+ +/- -/-
5 mm
B
P21 testis
Trip13 +/+ +/- -/-
TRIP13
SYCP3
ACTB
C
p=0.0001
p=0.0211
Testis / body weight ratio
0.008
0.006
0.004
0.002
0.000
Trip13+/+
Trip13+/-
Trip13-/-
D
x10^7
p=0.0001
p=0.0045
Sperm count
2.0
1.5
1.0
0.5
0.0
Trip13+/+
Trip13+/-
Trip13-/-
E
Trip13+/+
Dip
Sertoli
Zyg
eS
Trip13+/-
Sertoli
Dip
eS
Zyg
Trip13-/-
Sertoli
Pa-like
25 µm

Figure 2

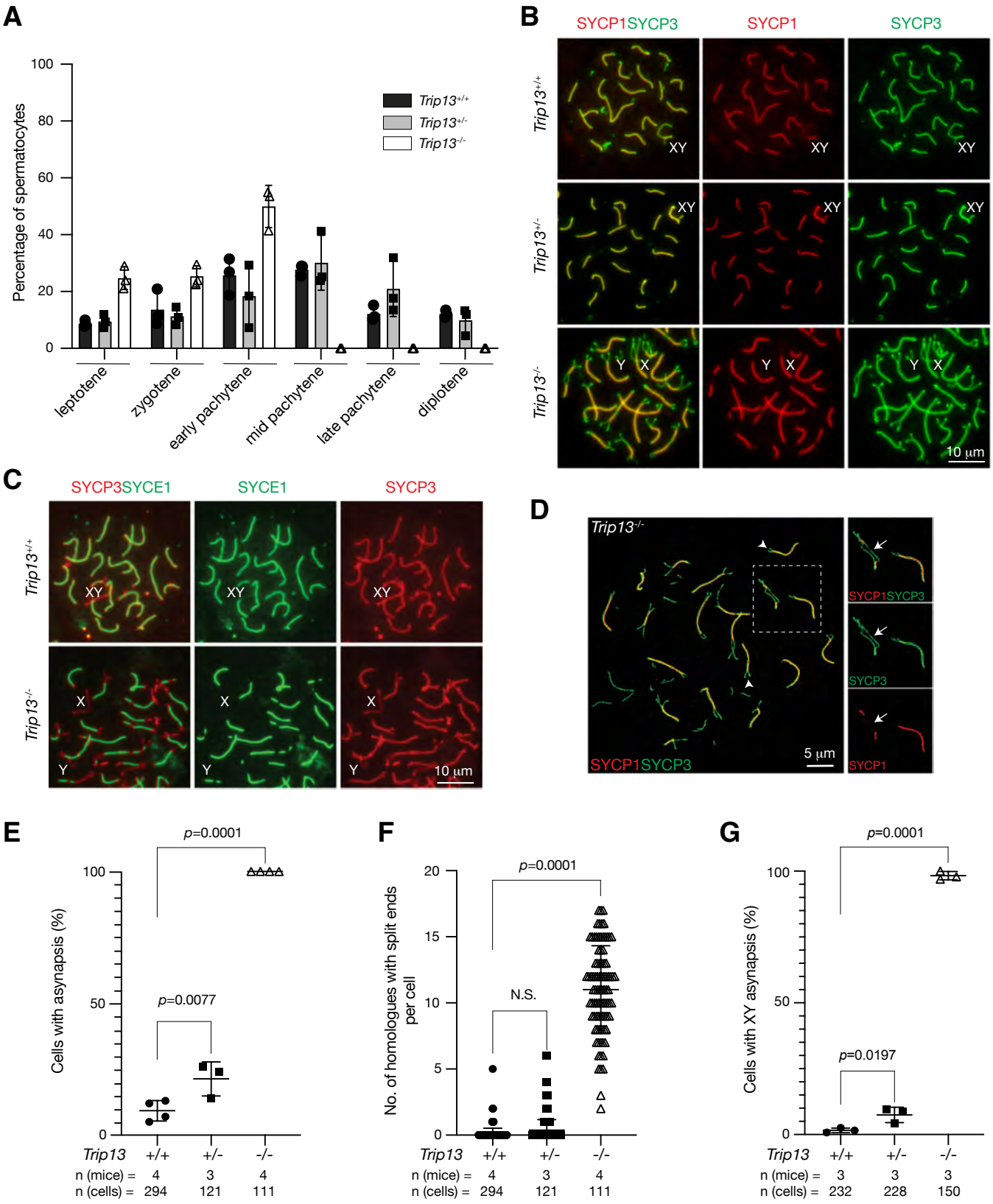
A
Percentage of spermatocytes
100
80
60
40
20
0
Trip13+/+
Trip13+/-
Trip13-/-
leptotene
zygotene
early pachytene
mid pachytene
late pachytene
diplotene
B
SYCP1SYCP3
SYCP1
SYCP3
Trip13+/+
Trip13+/-
Trip13-/-
XY
Y X
10 µm
C
SYCP3SYCE1
SYCE1
SYCP3
Trip13+/+
Trip13-/-
XY
X
Y
10 µm
D
Trip13-/-
SYCP1SYCP3
SYCP3
SYCP1
5 µm
E
p=0.0001
p=0.0077
Cells with asynapsis (%)
100
50
0
Trip13 +/+ +/- -/-
n (mice) = 4 3 4
n (cells) = 294 121 111
F
p=0.0001
N.S.
No. of homologues with split ends per cell
20
15
10
5
0
Trip13 +/+ +/- -/-
n (mice) = 4 3 4
n (cells) = 294 121 111
G
p=0.0001
p=0.0197
Cells with XY asynapsis (%)
100
50
0
Trip13 +/+ +/- -/-
n (mice) = 3 3 3
n (cells) = 232 228 150

Figure 3

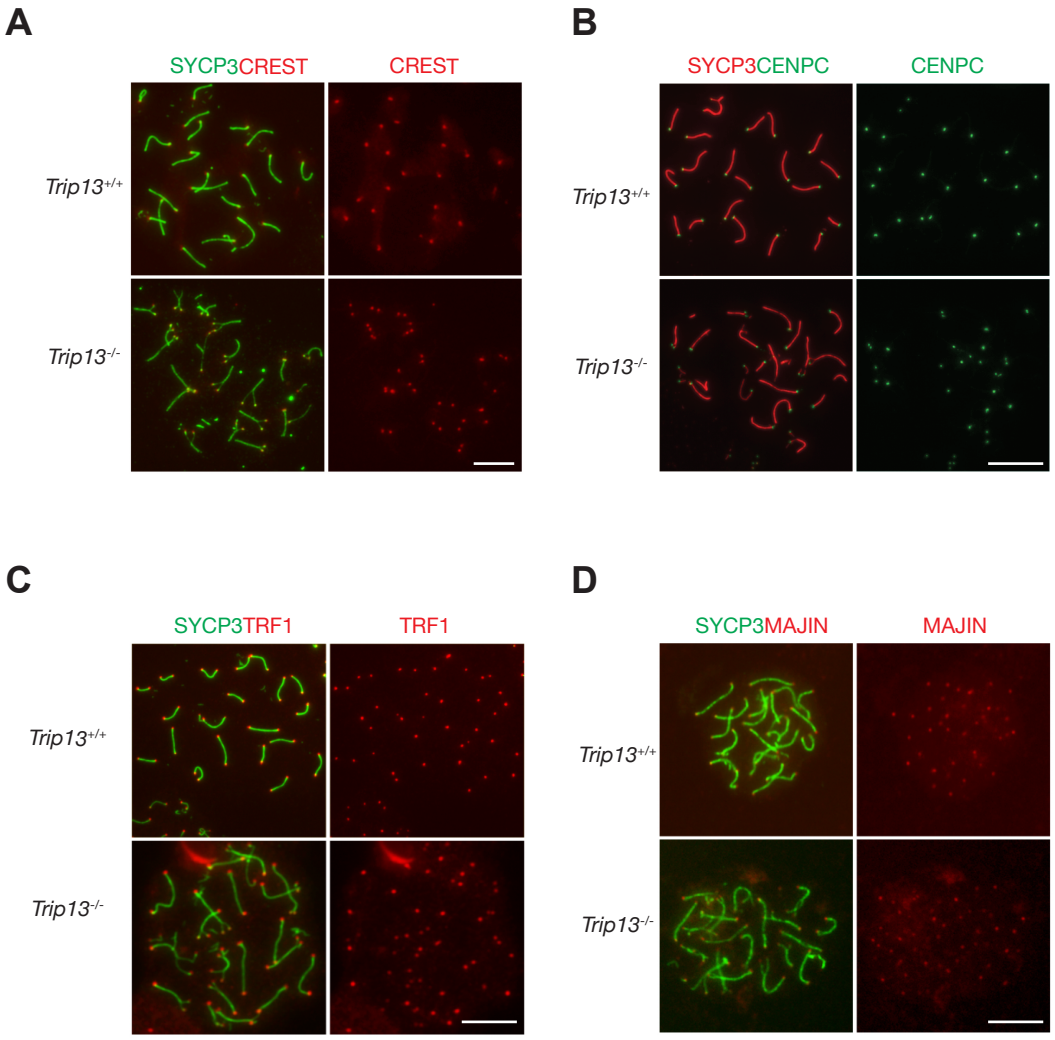
A
SYCP3CREST
CREST
Trip13+/+
Trip13-/-
B
SYCP3CENPC
CENPC
Trip13+/+
Trip13-/-
C
SYCP3TRF1
TRF1
Trip13+/+
Trip13-/-
D
SYCP3MAJIN
MAJIN
Trip13+/+
Trip13-/-

Figure 4

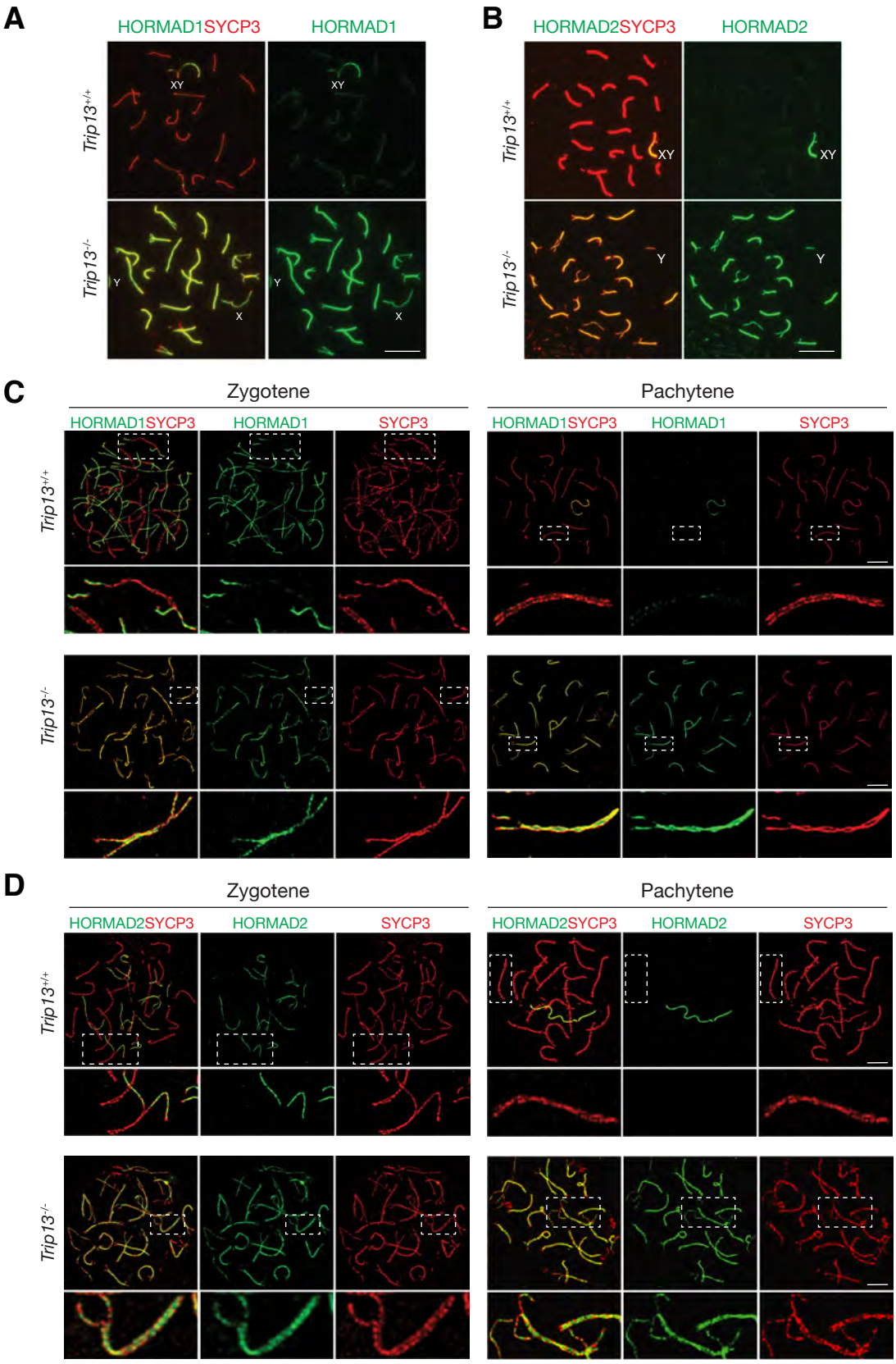
A
HORMAD1SYCP3
HORMAD1
Trip13+/+
Trip13-/-
XY
Y
X
B
HORMAD2SYCP3
HORMAD2
C
Zygotene
Pachytene
HORMAD1SYCP3
HORMAD1
SYCP3
D

Figure 5

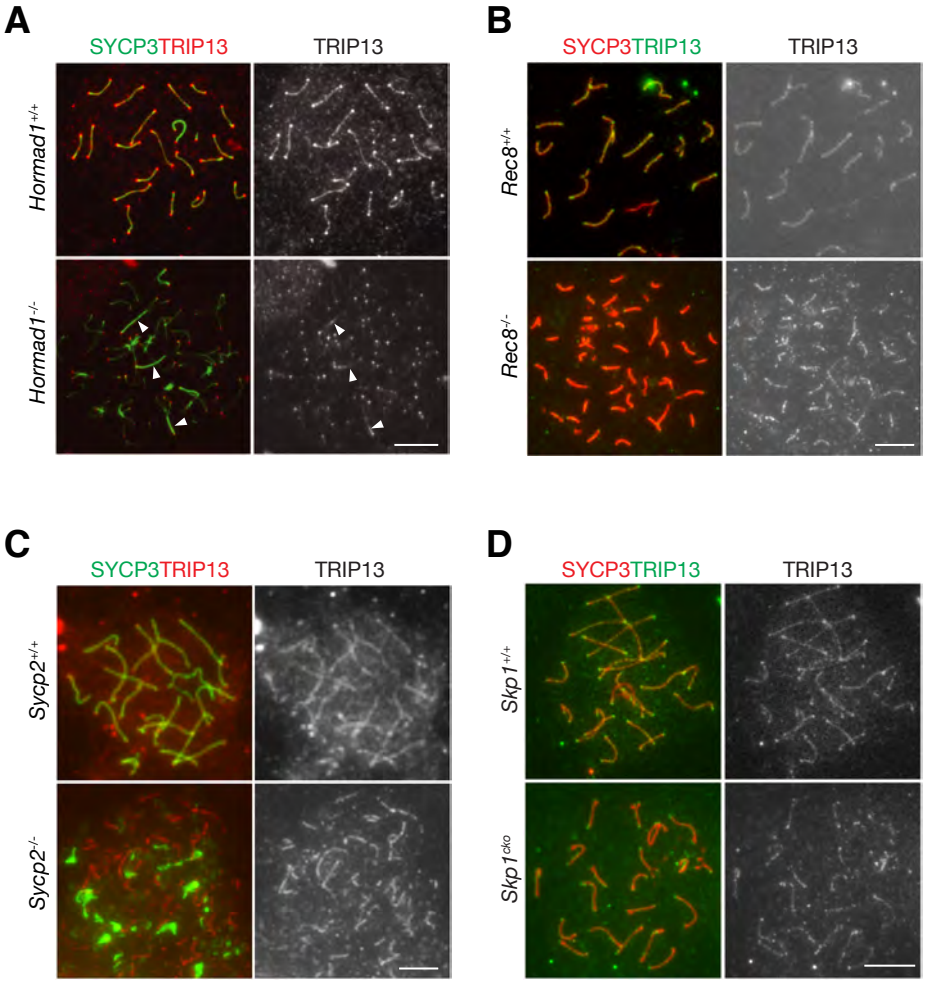
A
SYCP3TRIP13
TRIP13
Hormad1+/+
Hormad1-/-
B
SYCP3TRIP13
TRIP13
Rec8+/+
Rec8-/-
C
SYCP3TRIP13
TRIP13
Sycp2+/+
Sycp2-/-
D
SYCP3TRIP13
TRIP13
Skp1+/+
Skp1cko

Figure 6

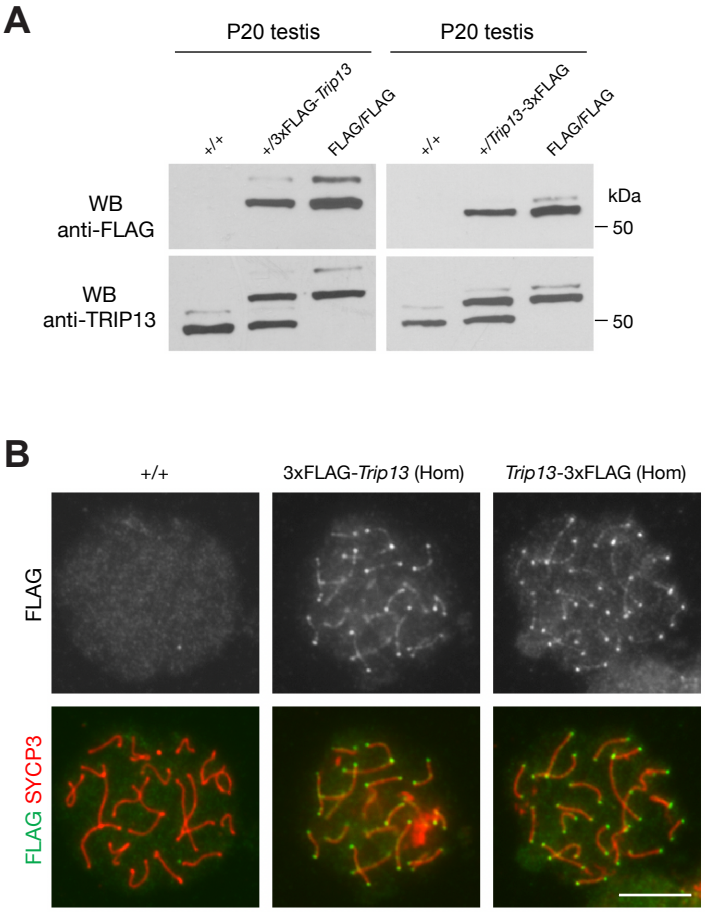
A
P20 testis
P20 testis
+/+
+/3xFLAG-Trip13
FLAG/FLAG
+/+
+/Trip13-3xFLAG
FLAG/FLAG
WB
anti-FLAG
WB
anti-TRIP13
kDa
50
50
B
+/+
3xFLAG-Trip13 (Hom)
Trip13-3xFLAG (Hom)
FLAG
FLAG SYCP3

Figure 7

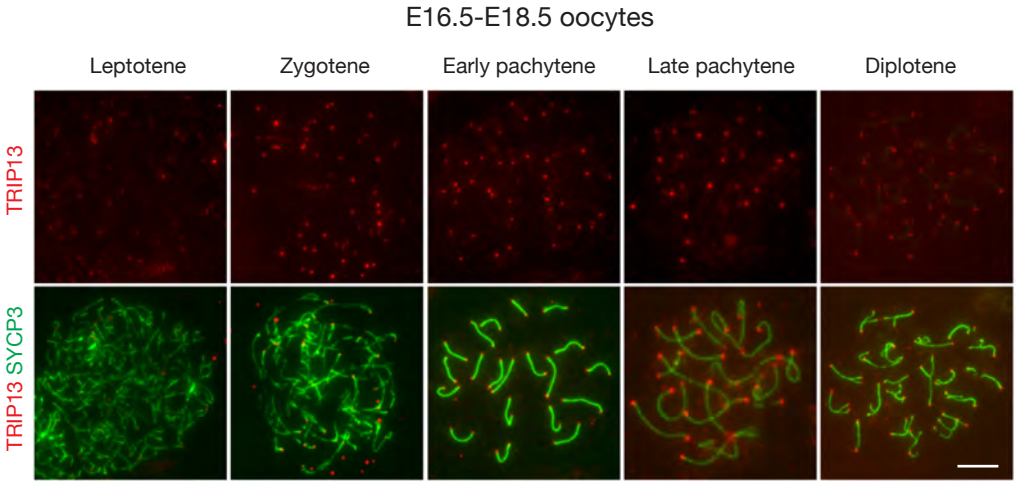

Figure 1 - supplement 1

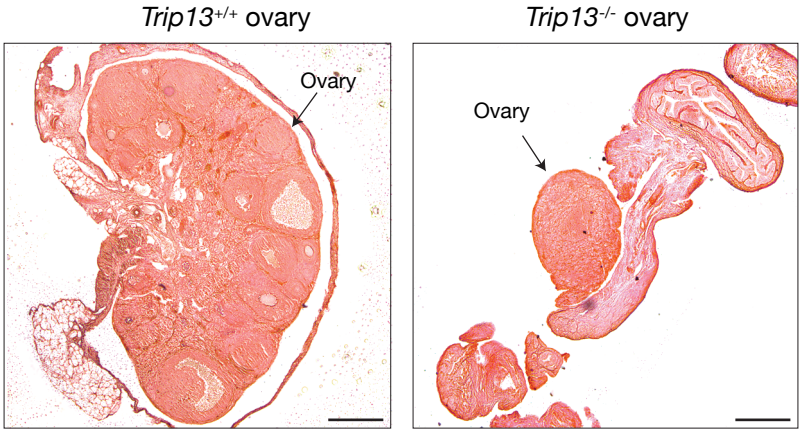

Figure 2 - supplement 1

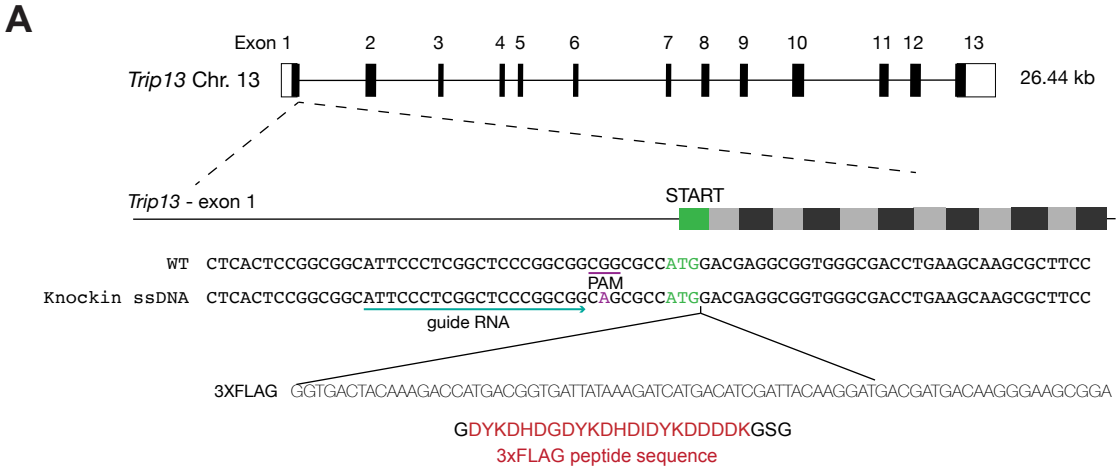

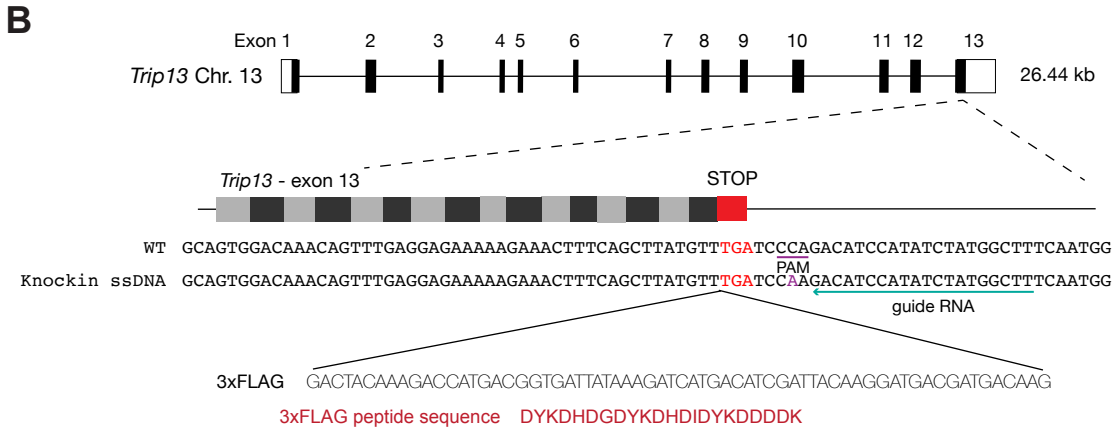

Figure 7 - supplement 1